Journal of
Synchrotron Radiation

ISSN 0909-0495

Received 21 March 2013
Accepted 5 July 2013

White-beam X-ray radioscopy and tomography with simultaneous diffraction at the EDDI beamline

F. García-Moreno,[a,b] C. Jiménez,[a]* P. H. Kamm,[b] M. Klaus,[a] G. Wagener,[a] J. Banhart[a,b] and Ch. Genzel[a]

[a]Helmholtz-Zentrum Berlin, Hahn-Meitner-Platz 1, Berlin 14109, Germany, and [b]Technische Universität Berlin, Hardenbergstrasse 36, 10623 Berlin, Germany. E-mail: catalina.jimenez@helmholtz-berlin.de

A set-up for simultaneous imaging and diffraction that yields radiograms with up to 200 frames per second and 5.6 µm effective pixel size is presented. Tomograms and diffractograms are acquired together in 10 s. Two examples illustrate the attractiveness of combining these methods at the EDDI beamline for *in situ* studies.

Keywords: synchrotron X-ray imaging; energy-dispersive X-ray diffraction; *in situ* synchrotron diffraction; radioscopy; white-beam X-ray tomography.

EDDI (from Energy Dispersive DIffraction) is a multi-purpose beamline for materials research operated at the synchrotron facility BESSY II in Berlin, Germany (Genzel *et al.*, 2007). White beam (about 6–120 keV) is provided by a superconducting 7 T multipole wiggler. The energy-dispersive diffraction mode and the high photon flux make EDDI well suited for time-resolved *in situ* experiments. A high demand for both imaging and diffraction experiments motivated the construction of a set-up that offers both simultaneously (Fig. 1). Our first results using this set-up yielded radiograms with up to 200 frames per second (fps) and 5.6 µm effective pixel size, resulting in the acquisition of whole tomograms and respective entire diffractograms in 10 s.

The cross section of the *incident* beam and thus the field of view for imaging at the sample are adjusted by opening the slit system S2 (see Fig. 1). For these experiments, S2 was opened to 4 mm × 2 mm (axial × equatorial = horizontal × vertical in the radiograms) but the largest possible cross section is 4 mm × 4 mm (Genzel *et al.*, 2007). After being partially absorbed by the sample, the *direct* transmitted X-ray beam is converted into visible light by a 200 µm-thick LuAG scintillator situated inside a cavity enclosed by a lateral Al frame wrapped by a 30 µm-thick Al foil and a bellow that makes it light-tight but almost X-ray transparent for the *diffracted beam* (in Fig. 1 the Al foil is indicated but not drawn in order to show the beam paths). After the scintillator, the light is mirrored by 90° and the image is magnified 2.3 times by a macro-lens and extension tubes, after which it is recorded by a fast PCO1200 CMOS camera (1280 × 1024 pixels, 12 µm × 12 µm pixel size). The rotation table for tomography is a Huber one-circle goniometer (model 408) that allows 2000 projected radiograms to be acquired in 10 s for one full rotation. Without being attenuated by any component of the set-up except twice by the Al foil, the cross section and angular divergence of the *diffracted* X-ray beam are adjusted by opening the slit systems S3 and S4, usually within the range 5–10 mm × 0.01–0.03 mm (axial × equatorial) and for these experiments 5 mm × 0.01 mm. After being collimated by S3 and S4, the diffracted beam is recorded by a multi-channel germanium analysing detector (Canberra model GL0110) at a fixed 2θ angle aligned in the vertical plane of the incident beam axis [for further

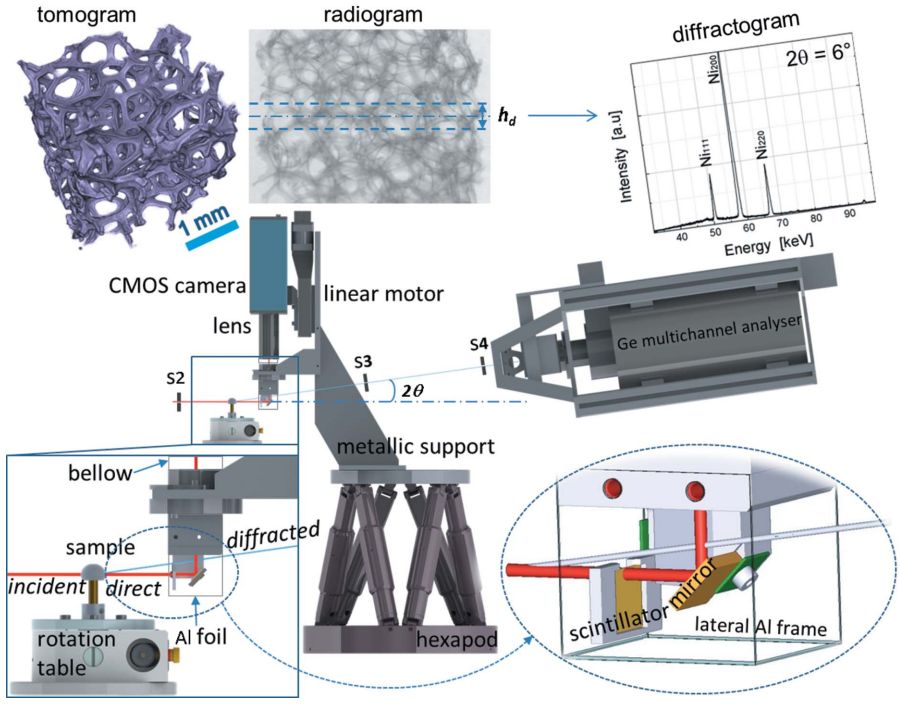

Figure 1
Set-up for combined X-ray radioscopy or tomography with simultaneous energy-dispersive diffraction at the EDDI beamline. This example shows the simultaneous acquisition of the tomogram and diffractogram of an open-cell Ni-based foam (Alantum Europe) in 10 s and the three-dimensional reconstruction. The dashed lines in the radiogram indicate the location and height of the projected region h_d analysed by diffraction.

details see Genzel *et al.* (2007)]. In these experiments, 2θ was 6° but for the present set-up it can be arbitrarily selected between 2° and 14°. A hexapod and a linear (vertical) motor connected to each other by a metallic support (designed to be beside the diffracted beam path) are used for positioning and fine-focusing, respectively. Both tomogram and diffractogram of the open-cell Ni-based foam shown in Fig. 1 were acquired at ambient temperature in 10 s. The dashed lines above and below the half-height of the radiogram indicate the projected height analysed by diffraction h_d, where $h_d \cong t\tan(2\theta) + eq_{S3}/\cos(2\theta)$, with t the sample thickness and eq_{S3} the equatorial opening of S3.

Diffraction data can be analysed on-line using self-developed tools based on *Mathematica* (Genzel *et al.*, 2007). Radiograms are background-corrected using the software *ImageJ* or *Fiji*. Tomographic reconstructions are obtained with *Octopus 8.6*. The program *VGStudio Max* is used for visualization of three-dimensional data, *Avizo* and *Mavi* for three-dimensional image analyses. Quantitative two-dimensional image analyses are performed with self-developed Matlab codes and the software *Axim* (García-Moreno *et al.*, 2004).

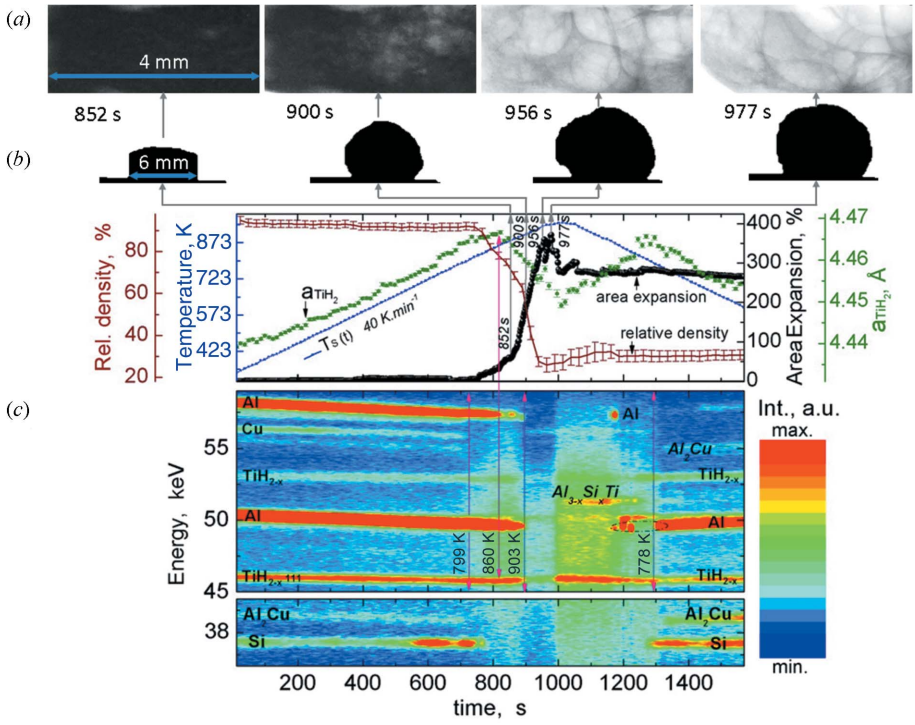

Figure 2
(*a*) Synchronized radiograms, (*b*) corresponding binary images and (*c*) time–temperature-dependent map of diffracted intensities acquired *in situ* during foaming of the powder alloy AlSi6Cu4 with 5 wt% of the blowing agent TiH_{2-x}.

Radioscopy and diffraction at EDDI were applied simultaneously to study *in situ* the dynamic process of metal foaming (Jiménez *et al.*, 2013). For this, the rotation table shown in Fig. 1 was exchanged for a heating plate on which the sample does not rotate but experiences structural changes and phase transformations induced by heating, which are monitored *in situ* by radioscopy and diffraction, respectively. In Fig. 2 the foaming process of AlSi6Cu4 compacted alloy powder containing 5 wt% of the blowing agent TiH_{2-x} is presented. The sequence of selected radiograms in Fig. 2(*a*) reveals the internal evolution of the foam structure and yields the relative density of the foam [calculated according to García-Moreno *et al.* (2009, 2011)] during the thermal cycle $T_S(t)$ measured at the sample bottom. Fig. 2(*b*) shows respective binary images of the entire foam, which were recorded by a video camera from which the overall area foam expansion was calculated. The synchronized map of diffracted intensities in Fig. 2(*c*) exhibits the principal lines of all crystalline phases and discloses individual phase transformations. There is liquid metal above 799 K on heating and 778 K on cooling denoted by the diffuse scattering that increases the background level as the diffraction lines of Si, Al, Cu and Al_2Cu fade. The time and temperature dependence of the lattice parameter $a_{TiH_{2-x}}$ of the blowing agent was calculated by sequential fitting of the principal line (111) of TiH_{2-x} that allowed $d_{111} \propto \text{constant}/E_{111}$ to be determined and then $a_{TiH_{2-x}}$ through the formula $a_{TiH_{2-x}} = 3^{1/2} d_{111}$ (Jiménez *et al.*, 2011). Lattice parameter contraction above 860 K during heating indicates that TiH_2 decomposes while releasing H_2 gas that expands the liquid metal (Jiménez *et al.*, 2011, 2013).

Application of these combined methods appears especially attractive for any *in situ* study of dynamic processes in materials that simultaneously undergo phase transformations and localized structural transformations, such us metal foaming. For other *in situ* experiments (not included here), heating stages under controlled atmosphere and a tension–compression mechanical testing device are also available at the beamline. Possible applications include sintering, welding, density or volume changes, diffusion and material transport, grain growth, crack growth, fracture, *etc*. Therefore, this option is readily offered to all EDDI users and in the near future we aim to improve the time and the effective pixel size to between 500–1000 fps and 2–3 µm, respectively.

References

García Moreno, F., Fromme, M. & Banhart, J. (2004). *Adv. Eng. Mater.* **6**, 416–420.
García-Moreno, F., Jiménez, C., Mukherjee, M., Holm, P., Weise, J. & Banhart, J. (2009). *Colloid Surface A*, **344**, 101–106.
Garcia-Moreno, F., Solórzano, E. & Banhart, J. (2011). *Soft Matter*, **7**, 9216.
Genzel, Ch., Denks, I., Gibmeier, J., Klaus, M. & Wagener, G. (2007). *Nucl. Instrum. Methods Phys. Res. A*, **578**, 23–33.
Jiménez, C., Garcia-Moreno, F., Pfretzschner, B., Kamm, P. H., Neu, T. R., Klaus, M., Genzel, C., Hilger, A., Manke, I. & Banhart, J. (2013). *Adv. Eng. Mater.* **15**, 141–148.
Jiménez, C., Garcia-Moreno, F., Pfretzschner, B., Klaus, M., Wollgarten, M., Zizak, I., Schumacher, G., Tovar, M. & Banhart, J. (2011). *Acta Mater.* **59**, 6318–6330.